On the Coronal Magnetic Field Configuration and Solar Flare/CME Process

Yihua Yan
National Astronomical Observatories, Chinese Academy of Sciences, Beijing 100012, China

for the special issue of HPC2005, August 1, 2005

Abstract. The coronal magnetic field configuration is important for understanding the energy storage and release processes that account for flares and/or CMEs. Here we present a model which is based on the work for potential magnetic field problems that only applies the condition at infinity with the boundary condition on the solar surface specified. We also discuss some recent progress on general force-free field models. For some event analyses, we have employed MDI/SOHO longitudinal magnetogram insected into the synoptic magnetogram to obtain whole boundary condition over the solar surface. Globally, the extrapolated global magnetic field structures effectively demonstrate the case for the disk signature of the radio CMEs and the evolution of the radio sources during the CME/flare processes.

Keywords: Sun:magnetic fields—Sun:flares—Sun:corona

1. Introduction

It is generally accepted that the magnetic fields actually control all physical processes and observed phenomena in the solar corona. The corona is characterized by highly inhomogeneous ensemble of loop structures, coronal holes and X-ray bright points. Many dynamic processes such as upflows and heating of coronal plasma are driven by the solar magnetic fields (Aschwanden, 2004). Consequently, coronal images in EUV/UV and/or SXR wavelengths are used to diagnose coronal magnetic structures. The loop or thread-like structures shown in EUV/UV and/or SXR are believed to resemble the coronal magnetic field. With assumptions on radiation mechanisms and propagations, radio techniques can be applied to diagnose the coronal field. Direct measurement of the coronal magnetic field is possible (e.g., Lin et al., 2000), but not well-established yet for space weather applications. At present reliable magnetic field measurements are confined to the photosphere and extrapolation from observed photospheric data upwards is still the primary tool to reconstruct coronal magnetic field (Yan, 2003).

Coronal field configurations are important for understanding how energy is stored, triggered, released and transported in the flare/CME processes; how to support filaments/prominences and structures of CMEs; etc. In solar corona it can be considered as quasi-equilibrium evolution

with low β plasma. In practice, it is generally needed to construct global coronal field structure for CME analysis and local field for flares, active regions, etc. In reality, it is needed to obtain both local and global field structures so as to understand the trans-active region (or trans-equatorial) CMEs, associations of multiple waveband observations such as optical, hard X-ray (HXR) and radio source, etc (Wang et al., 2002).

The simplest 3D magnetic field model is quantified in terms of a potential field, which is often used to compute the coronal field with a source-surface model. In this case the source-surface is employed to fit the observed coronal structures and free parameters are needed in order to obtain closed field region versus open field lines (Hoeksema and Scherrer, 1986; Zhao and Hoeksema, 1994). Here we introduce the BIE (boundary integral equation) solution for potential problem (Yan et al., 1993) which has been used recently for solar coronal field (e.g., Wang et al., 2002; Yan, 2005). By BIE formulation the observed line-of-sight boundary data are employed directly and only the asymptotic condition of no field at infinity is employed. Therefore no free parameter is needed and the solution is unique. A physically better motivated approach is the framework of force-free fields, where the Lorentz force on a magnetic field vanishes as it can be justified in the low-β corona (Aschwanden, 2004; Yan, 2003). Different methods for non-constant-α force-free magnetic field have been summarized recently in Aschwanden (2004) and the BIE model can take into account the finite energy content in open space and implement the vector boundary data directly (Yan and Sakurai, 1997, 2000). In principle, the BIE method can obtain global field from observed boundary data, but due to the lack of global vector magnetic field measurements, which are only available for active regions at present, the method has been applied to active regions for solar activities (e.g., see discussions in Yan, 2003). Since normal differential of the field on the boundary has to be solved numerically in the BIE formulation, a dense algebraic coefficient matrix is usually encountered. Here we present an improved formulation for the elimination of this differential term for a simple geometry of the semi-space (Yan and Li, 2006) or a sphere (Li et al., 2005). We may expect future space or ground based observations for whole disk vector magnetograms in order to apply the BIE model for space weather applications. Finally we present two event analyses with the comparisons of reconstructed global potential field configuration by the proposed method and observed HXR and radio images, so as to understand the flare and CME initial processes.

2. Coronal Magnetic Field Model

2.1. Direct boundary integral equation for non-constant-α force-free field

Following Yan and Sakurai (1997; 2000), the equations describing a force-free magnetic field in the region Ω can be obtained as follows.

$$\bigtriangledown \times \mathbf{B} = \alpha \mathbf{B}, \tag{1}$$

$$\bigtriangledown \cdot \mathbf{B} = 0, \tag{2}$$

where α is a function of spatial location and is determined consistently from the boundary conditions since it is constant along field lines. It is further assumed that both α and $\bigtriangledown\alpha$ are bounded.

The boundary condition over a region on Γ is

$$\mathbf{B} = \mathbf{B}_o. \tag{3}$$

$\mathbf{B}_o$ here denotes known boundary values which must be prescribed consistently.

Physically the magnetic field should tend to zero identically at infinity. Therefore an asymptotic condition which ensures a finite energy content in semi space above the Sun (Yan and Sakurai, 1997, 2000) is employed,

$$\mathbf{B} = O(R^{-2}), \quad \text{when} \quad R \to \infty. \tag{4}$$

A similar treatment to Yan and Sakurai (2000), which follows that in classical exterior boundary value problems (Stratton, 1941;Courant and Hilbert, 1962, etc.), gives the following results (Yan and Li, 2006). A direct boundary integral formulation for the solution of the exterior boundary value problem (1-4) under the semi-space geometry with $\Gamma = \{(x, y, z)|z = 0\}$ and $\Omega = \{(x, y, z)|z > 0\}$ can be expressed as follows,

$$\mathbf{B}(\mathbf{r_i}) = -\int_\Gamma \frac{\partial Y(\mathbf{r}; \mathbf{r}_i, \lambda)}{\partial n} \mathbf{B}_0(\mathbf{r}) d\Gamma, \tag{5}$$

in which $n = -z$, $\mathbf{r} = (x, y, z)$, $\mathbf{r}_i = (x_i, y_i, z_i)$, and $\lambda = \lambda(\mathbf{r}_i)$ is a pseudo force-free factor to be determined by the following formula,

$$\int_\Omega Y(\mathbf{r}; \mathbf{r}_i, \lambda)[\lambda^2 \mathbf{B} - \alpha^2 \mathbf{B} - \bigtriangledown\alpha \times \mathbf{B}] d\Omega = 0, \tag{6}$$

where,

$$Y = Y_1 - Y_2, \quad \text{with,} \quad Y_1 = \frac{\cos(\lambda|\mathbf{r} - \mathbf{r}_i|)}{4\pi|\mathbf{r} - \mathbf{r}_i|}, \quad Y_2 = \frac{\cos(\lambda|\mathbf{r} - \mathbf{r}_{im}|)}{4\pi|\mathbf{r} - \mathbf{r}_{im}|}, \tag{7}$$

in which $\mathbf{r}_{im} = (x_i, y_i, -z_i)$ is the mirror point of the fixed point with respect to the boundary Γ (Yan and Li, 2006). It has been evaluated against a closed form solution that such pseudo force-free factor λ's in the Yan and Sakurai (2000) formulation do exist (Li et al., 2004). The reference function Y satisfies the following equation,

$$\bigtriangledown^2 Y + \lambda^2 Y = \delta_i \ \text{ in } \ \Omega, \quad \text{with } \ Y = 0 \ \text{ on } \ \Gamma, \tag{8}$$

where δ_i is the Dirac function defined at the point, $i \in \Omega$.

In the case that the boundary is a spherical geometry with $\Gamma = \{(x, y, z)|r = |\mathbf{r}| = R_\circ\}$ and $\Omega = \{(x, y, z)|r = |\mathbf{r}| > R_\circ\}$, with $R_\circ$ as solar radius, a similar derivation leads to the following result,

$$\mathbf{B}(\mathbf{r}_i) = -\int_\Gamma \frac{\partial Y(\mathbf{r}; \mathbf{r}_i, \lambda)}{\partial n} \mathbf{B}_0(\mathbf{r}) d\Gamma, \tag{9}$$

in which $n = -r$ and,

$$Y = Y_1 - Y_2, \ \text{ with, } \ Y_1 = \frac{\cos(\lambda|\mathbf{r} - \mathbf{r}_i|)}{4\pi|\mathbf{r} - \mathbf{r}_i|}, \ Y_2 = \frac{\cos(\lambda \frac{r_i}{R_\circ}|\mathbf{r} - \mathbf{r}_{im}|)}{4\pi \frac{r_i}{R_\circ}|\mathbf{r} - \mathbf{r}_{im}|} \tag{10}$$

where the mirror point of the fixed point with respect to the boundary Γ becomes $\mathbf{r}_{im} = \frac{R_\circ^2}{r_i^2}(x_i, y_i, z_i)$ (Courant and Hilbert, 1962). The pseudo-force-free factor $\lambda = \lambda(x_i, y_i, z_i)$ now has to be determined from a different equation as follows (Li et al., 2005),

$$\int_\Omega \{Y(\mathbf{B} \times \bigtriangledown \alpha - \alpha^2 \mathbf{B}) + \lambda^2 \mathbf{B}[Y_1 - (\frac{r_i}{R_\circ})^2 Y_2]\} d\Omega = 0, \tag{11}$$

and the reference functions satisfies the following equation instead (Li et al., 2005),

$$\bigtriangledown^2 Y_1 + \lambda^2 Y_1 = \delta_i, \ \ \bigtriangledown^2 Y_2 + (\lambda \frac{r_i}{R_\circ})^2 Y_2 = 0 \ \text{ in } \ \Omega, \ \text{ with } \ Y = 0 \ \text{ on } \ \Gamma. \tag{12}$$

In principle, the BIE method can construct global coronal field from observed magnetogram, but the vector magnetic fields are needed in the boundary conditions which are not available globally at present. We may expect future space or ground based observations for whole disk vector magnetograms in order to apply the BIE model for space weather applications. Nevertheless, the BIE method (Yan and Sakurai,1997, 2000) has been applied to the reconstruction of coronal magnetic field above active regions for solar activities. For example, for the first time a flux rope structure was inferred from the observed boundary data (Yan et al. 2001a, 2001b) for the famous 2000 Bastille-day event (e.g., see more applications of the method in Yan, 2003). In the next section we

will introduce the BIE solution for potential problem with the observed line-of-sight boundary data employed directly.

2.2. Boundary integral equation for global potential field

The source-surface is generally employed to reconstruct the coronal field configuration by fitting the observed coronal structures and a free parameter is needed in order to obtain closed field region versus open field lines for the source-surface method or its variants (Hoeksema and Scherrer, 1986; Zhao and Hoeksema, 1994). The Green's function methods and the eigen function expansion methods are normally used in solar physics (Sakurai, 1989; Aschwanden, 2004).

Here the extrapolation code is based on the work for potential magnetic field problems (Yan et al., 1993) which was recently applied in solar physics (Wang et al., 2002; Yan, 2005). For the potential condition, which is governed by $\bigtriangledown \times \mathbf{B} = 0$ and $\bigtriangledown \cdot \mathbf{B} = 0$, the magnetic field can be represented by a scalar potential Ψ with $\mathbf{B} = - \bigtriangledown \Psi$. Then we have the Laplacian equation.

$$\bigtriangledown^2 \Psi = 0. \tag{13}$$

On the solar surface Γ we have line-of-sight field component or its normal component B_n specified, i.e.,

$$B_n = -\frac{\partial \Psi}{\partial n}. \tag{14}$$

Therefore we can obtain a boundary value problem of (13-14), e.g., as described in Sakurai (1989), or Aschwanden (2004). In general, with the asymptotic condition of no field at infinity, the potential Ψ at any position $\mathbf{r}_i$ in space Ω can be determined from (Courant and Hilbert, 1962):

$$\Psi(\mathbf{r}_i) = \oint_\Gamma \left[G(\mathbf{r};\mathbf{r}_i) \frac{\partial \Psi(\mathbf{r})}{\partial n} - \frac{\partial G(\mathbf{r};\mathbf{r}_i)}{\partial n} \Psi(\mathbf{r}) \right] d\Gamma \tag{15}$$

where $G = 1/4\pi|\mathbf{r} - \mathbf{r}_i|$ is Green's function of Laplacian equation in free space. The Green's function solution of the above boundary value problem was applied to practical solar magnetic field observations in early 1960s (Sakurai, 1989). Here, the magnetic field is, however, obtained from:

$$\mathbf{B}(\mathbf{r}_i) = \oint_\Gamma \left[\Psi \frac{\partial}{\partial r} \left(\frac{\partial G}{\partial n} \right) - \frac{\partial \Psi}{\partial n} \frac{\partial G}{\partial r} \right] \frac{\mathbf{r}_i - \mathbf{r}}{|\mathbf{r} - \mathbf{r}_i|} d\Gamma \tag{16}$$

with $\partial\Psi/\partial n$ known over the boundary and Ψ solved numerically by the boundary element method (Yan et al., 1993), which is a well-established method for science and technology applications (Brebbia

et al., 1984). The model here actually deals with an exterior Neumann problem of the Laplacian equation, which has a unique solution if it exists (Courant and Hilbert, 1962). In this case the boundary data must be flux balanced and the field tends to zero at infinity. However, for the source-surface model one actually introduces the degree of freedom leading to various heights of the source surface. If the data are given that satisfy the flux balance, still one can impose how much of the flux is open, and one degree of freedom will be left at one's discretion.

3. Results and Discussions

For the event analysis, we have employed MDI/SOHO longitudinal magnetogram inserted into the synoptic magnetogram to obtain whole boundary condition over the solar surface. Due to the projection effect, we employed MDI magnetogram data in the central region of $\pm 50^\circ$ longitude and $\pm 50^\circ$ latitude and the MDI synoptic magnetogram data in the regions of -180° to -50° and 50° to 180° longitude, and $\pm 60^\circ$ latitude.

3.1. 05-November-1998 event

The detailed analysis for the 05-November-1998 flare event at 13:34 UT is presented in Trottet et al. (2005). Here we only demonstrate the associations between the reconstructed coronal magnetic field structure and multi-wave band observations.

The observations show that at 13:34 UT the HXR sources and radio sources from high frequency to low frequency are roughly orientated along the same direction, which agrees with the scenario of type III burst, or the ejection of electron beams along open field lines. But 1 minute later, the orientation of the radio burst sources from high frequency to low frequency were not located along the same direction with the HXR source on the extension of the alignment. We have reconstructed the global coronal field with the above potential solution by BEM, and Figure 1 displays the results for some selected open and closed field lines. It shows that the radio sources are located in divergent fan-like magnetic field structures with HXR source, observed by Yohkoh, connected to this fan-like region. From projected field lines (Figure 1a) we do not see a direct field lines connecting radio sources, observed by Nancay Radioheliograph (NRH), to HXR sources. If, however, we assume the altitude of radio sources are in a range of about 1.1-1.5 solar radius, as shown in Figure 1b, we do see that radio sources at 432 and 410 MHz are connected to the HXR source

region by closed field lines and they are not in the same open field lines connecting radio sources at lower frequencies. For burst pattern at 12:34 UT, there might be direct injections from HXR source to the fan-like region and somehow these electrons are ejected along open lines as type III bursts. For burst pattern at 13:35 UT, as shown in Figure 1c, we do not get field lines that connect radio sources and HXR sources directly. However, the side view of the radio sources (as shown in Figure 1d) indicates that they are in the same fan-like cusp region. It must be noted that the altitudes of those radio sources are highly uncertain because they are obtained based on the plasma mechanism for type III bursts. Nevertheless, the reconstructed magnetic field configuration provide possible explanation for those radio sources to locate.

3.2. 17-Mar-2002 event

For the 17-Mar-2002 event, the detailed analysis for the CME process and the associations with the NRH radio sources is presented elsewhere (Wang et al., 2005). Figure 2 shows the radio sources overlaid on Hα image and Figure 3 shows the reconstructed coronal field configuration.

The extrapolated global magnetic field structures effectively demonstrate the case for the disk signature of the radio CME and the evolution of the radio sources during the CME/flare processes. It is obtained that the radio counterpart of the CME as well as source of type III burst were propagating along the open field lines. The result shows that the extrapolated field structures are very helpful to understand the flare/CME process.

4. Conclusions

Reconstructed coronal field configurations can effectively demonstrate the multi-wavelength observations for flare/CME events. It is expected that global vector magnetogram on solar surface be measured. Efforts to combine both large-scale and small-scale field are needed and fast computing techniques should be developed for space weather applications.

Acknowledgements

The work was supported by National Natural Science Foundation of China (10225313, 10333030), Chinese Academy of Sciences and the Ministry of Science and Technology of China (G2000078403). Drs. Wang

M., Pick M. and Trottet G. are acknowledged for the event analysis involved and Ph.D. student Li Z. for assistance. Yohkoh, SOHO/MDI and NRH data have been used in the present study.

References

Aschwanden, M. J.: 2004, *Physics of the Solar Corona*. Springer-Verlag.
Brebbia, C. A., Telles, J. C. F. and Wrobel, L. C.: 1984, *Boundary Element Techniques*. Springer-Verlag
Courant, R., and Hilbert, D.: 1962, *Methods of Mathematical Physics, Vol. II*. Interscience Publishers
Hoeksema, J. T. and Scherrer, P. H.: 1986, Sol. Phys. 105, 205
Li, Z., Yan, Y., Song, G.: 2004, MNRAS, 347, 1255
Li, Z., Yan, Y., Song, G.: 2005, Journal of Xidian University, in press (in Chinese)
Lin, H.S., Penn, M. J., Tomczyk, S.: 2000, ApJ, 541, 83
Sakurai, T.: 1989, Space Sci. Rev. 51, 11
Stratton, J. A. 1941, *Electromagnetic Theory*. McGraw-Hill
Trottet, G., Correia, E., Karlicky, M., Aulanier, G., Yan, Y., Kaufmann, P.: 2005, Sol. Phys., submitted
Wang, T., Yan, Y., Wang, J., Kurokawa, H., Shibata, K.: 2002, ApJ, 572, 580
Wang, M., Pick, M., Yan, Y.: 2005, in preparation
Yan, Y.: 2003, Space Sci. Rev., 107, 119
Yan, Y.: 2005, in K. Dere, J. Wang and Y. Yan (eds.), *Coronal and Stellar Mass Ejections*. IAU Symp. No. 226, 277.
Yan, Y., Aschwanden, M. J., Wang, S., and Deng, Y.: 2001a, Sol. Phys., 204, 15
Yan, Y., Deng, Y., Karlický, M., Fu, Q., Wang, S., and Liu, Y. 2001b, ApJ, 551, L115
Yan, Y., and Li, Z.: 2006, ApJ, April 20 issue (in press)
Yan, Y., and Sakurai, T.: 1997, Sol. Phys., 174, 65
Yan, Y., and Sakurai, T.: 2000, Sol. Phys., 195, 89
Yan, Y., Yu, Q., and Shi, H.: 1993, in J. H. Kane, G. Maier, N. Tosaka and S. N. Atluri (eds.), *Advances in Boundary Element Techniques*. Springer-Verlag, 447
Zhao, X.P. & Hoeksema, J. T.: 1994, Sol. Phys. 151, 91

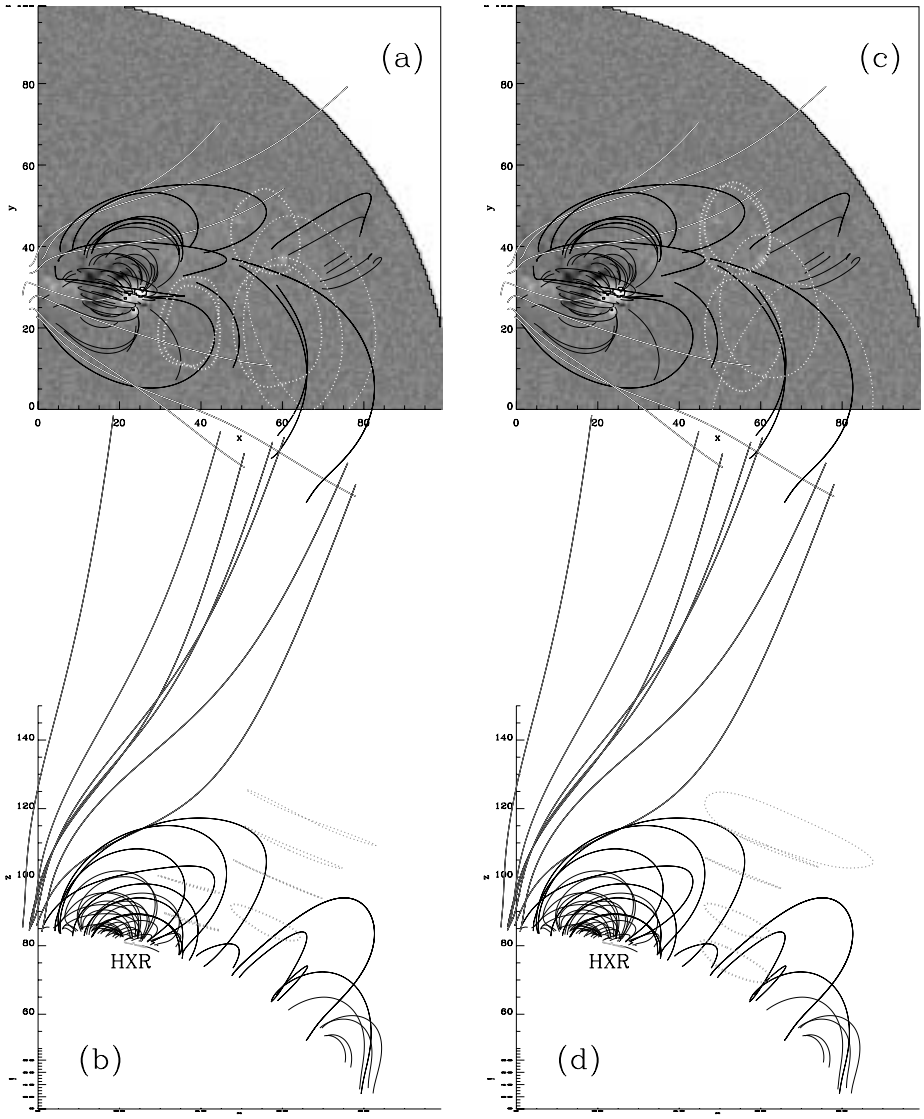

Figure 1. (a) Some selected open (solid white) and closed (solid black) field lines overlaid on line of sight magnetogram (greyscale with black/white = ±600 G) taken at 12:48 UT by SOHO/MDI. Patterns of Radio bursts by the NHR at 432, 410, 327, 236 and 164 MHz at 13:34 UT are also displayed by dotted contours in an order of increasing size and deceasing line thickness with 50% of the maximum brightness of the radio image. (b) The pattern of (a) viewed from front. The radio sources schematically locate at corresponding ranges. (c) The same as (a) but for radio burst patterns at 13:35 UT. (d) The pattern of (c) viewed from front.

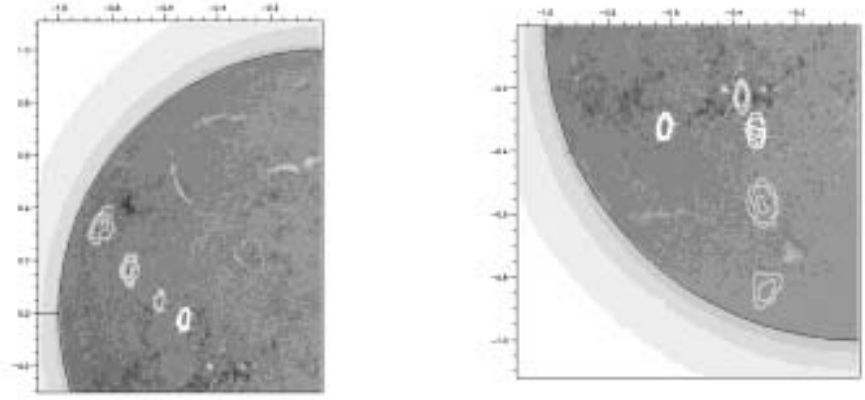

Figure 2. (a) Radio bursts by the NHR at 410, 327, 236 and 164 MHz at 09:57:21 UT are displayed by contours in an order of increasing size and deceasing line thickness and overlaid on Hα image. (b) Radio burst patterns at 10:14:41 UT.

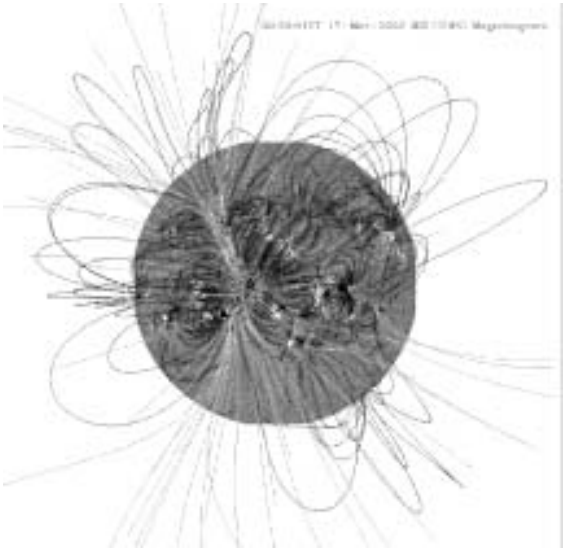

Figure 3. The reconstructed global magnetic field with SOHO/MDI magnetogram obtained at 09:39:01 UT shown in greyscale image.